frontiers | Frontiers in Surgery

TYPE Original Research
PUBLISHED 31 August 2022
DOI 10.3389/fsurg.2022.967399

OPEN ACCESS

EDITED BY
Sravisht Iyer,
Hospital for Special Surgery, United States

REVIEWED BY
Wen Yuan,
Shanghai Changzheng Hospital, China
Dingjun Hao,
Xi'an Honghui Hospital, China

*CORRESPONDENCE
Jing-Chi Li
lijingchi9405@163.com
Zhi-Peng Xi
xizhipeng1985@163.com

†These authors have contributed equally to this work and share first authorship

SPECIALTY SECTION
This article was submitted to Orthopedic Surgery, a section of the journal Frontiers in Surgery

RECEIVED 12 June 2022
ACCEPTED 15 August 2022
PUBLISHED 31 August 2022

CITATION
Huang C-Y, Zhang Z-F, Zhang X-Y, Liu F, Fang Z-X, Xi Z-P and Li J-C (2022) Poor bone mineral density aggravates adjacent segment's motility compensation in patients with oblique lumbar interbody fusion with and without pedicle screw fixation: An *in silico* study. Front. Surg. 9:967399. doi: 10.3389/fsurg.2022.967399

Poor bone mineral density aggravates adjacent segment's motility compensation in patients with oblique lumbar interbody fusion with and without pedicle screw fixation: An *in silico* study

Chen-Yi Huang[1†], Zi-Fan Zhang[2†], Xiao-Yu Zhang[3], Fei Liu[1], Zhong-Xin Fang[4], Zhi-Peng Xi[3*] and Jing-Chi Li[1,3*]

[1]Department of Orthopedics, Hospital (T.C.M) Affiliated to Southwest Medical University, Luzhou, China, [2]Department of Spine Surgery, Shanghai Changzheng Hospital, Naval Medical University, Shanghai, China, [3]Department of Orthopedics, Affiliated Hospital of Integrated Traditional Chinese and Western Medicine for Nanjing University of Chinese Medicine, Nanjing, China, [4]Fluid and Power Machinery Key Laboratory of Ministry of Education, Xihua University, Chengdu, China

Objective: Motility compensation increases the risk of adjacent segment diseases (ASDs). Previous studies have demonstrated that patients with ASD have a poor bone mineral density (BMD), and changes in BMD affect the biomechanical environment of bones and tissues, possibly leading to an increase in ASD incidence. However, whether poor BMD increases the risk of ASD by aggravating the motility compensation of the adjacent segment remains unclear. The present study aimed to clarify this relationship in oblique lumbar interbody fusion (OLIF) models with different BMDs and additional fixation methods.

Methods: Stand-alone (S-A) OLIF and OLIF fixed with bilateral pedicle screws (BPS) were simulated in the L4–L5 segment of our well-validated lumbosacral model. Range of motions (ROMs) and stiffness in the surgical segment and at the cranial and caudal sides' adjacent segments were computed under flexion, extension, and unilateral bending and axial rotation loading conditions.

Results: Under most loading conditions, the motility compensation of both cranial and caudal segments adjacent to the OLIF segment steeply aggravated with BMD reduction in S-A and BPS OLIF models. More severe motility compensation of the adjacent segment was observed in BPS models than in S-A models. Correspondingly, the surgical segment's stiffness of S-A models was apparently lower than that of BPS models (S-A models showed higher ROMs and lower stiffness in the surgical segment).

Abbreviations

AFD, additional fixation device; ASD, adjacent segment diseases; BEP, bony endplate; BMD, bone mineral density; BMI, body mass index; BPS, bilateral pedicle screw; CEP, cartilage endplate; DD, disc degeneration; FE, finite element; GB, grafted bone; HU, hounsfield unit; IVD, intervertebral disc; LDD, lumbar degenerative diseases; LIF, lumbar interbody fusion; OLIF, oblique lumbar interbody fusion; S-A, stand-alone; ROM, range of motion; ZJ, zygapophyseal joint.

Conclusion: Poor BMD aggravates the motility compensation of adjacent segments after both S-A OLIF and OLIF with BPS fixation. This variation may cause a higher risk of ASD in OLIF patients with poor BMD. S-A OLIF cannot provide instant postoperative stability; therefore, the daily motions of patients with S-A OLIF should be restricted before ideal interbody fusion to avoid surgical segment complications.

KEYWORDS

adjacent segment diseases, oblique lumbar interbody fusion, motility compensation, bone mineral density, finite elemant analysis

Introduction

Lumbar interbody fusion (LIF) surgeries are widely used to treat lumbar degenerative diseases (LDDs) (1, 2). Adjacent segment diseases (ASDs) are a common complication of spinal fusion surgery (3, 4). Motility compensation is an essential mechanism of biomechanical deterioration of the adjacent segment (5, 6). The stiffness of the interbody cage and grafted bone (GB) is higher than that of intervertebral disc (IVD) components. During LIF surgeries, the nucleus, cartilage endplates (CEPs), and parts of the annulus are replaced by the cage and GB (1, 7). Thus, the fusion segment shows higher stiffness than the original IVD. Consequently, the stiffness of the fusion segment is increased, and its range of motions (ROMs) is decreased under the same moments. ROMs of adjacent segments must be increased to achieve similar ROMs of the lumbar spine in different body positions (5, 6). This pathological process increases the risk of accelerated disc degeneration (DD) and instability in adjacent segments, leading to a poor prognosis for LIF patients (3, 4).

As mentioned above, biomechanical deterioration leads to an increased risk of developing ASDs (8, 9). According to surgeons, the demographic characteristics of patients with ASDs are closely related to certain types of biomechanical deterioration. Specifically, clinical follow-up studies have shown that patients with high body mass index (BMI) have a higher incidence of ASDs; correspondingly, biomechanical studies have confirmed that overweight patients have higher intradiscal pressure and annulus shear stress, which leads to annulus tear risk (3, 4). Elderly patients are at a greater risk of developing ASD; correspondingly, preexisting DD is confirmed as a risk factor for annulus stress concentration and further acceleration of DD (5, 10). Clinical studies have also shown that patients with osteoporosis have a higher risk of DD and ASD, but the biomechanical significance of poor bone mineral density (BMD) remains unclear (3, 4, 11).

Our previous study showed that poor BMD leads to stress concentration in adjacent segments; however, Zhang et al. reported a contrasting finding by using an approximate research method (8, 12). The indicator selected in both these studies was, however, limited to the stress distribution of IVDs, and there was a lack of explanation of how changes in BMD affect the motility compensation of the adjacent segment. Additional fixation devices (AFDs) are also commonly used to provide instant stability to the LIF segment (13, 14). The bilateral pedicle screw (BPS) is an extensively used AFD. Although BPS removal after interbody bone integration will alleviate biomechanical deterioration of the adjacent segment (5, 6, 15), no study has assessed whether the use of BPS aggravates motility compensation of the adjacent segments in the early postoperative period as compared to the stand-alone (S-A) surgical method (i.e., LIF without any AFD fixation).

On the basis of the abovementioned theoretical and practical knowledge, we hypothesize that poor BMD may cause a high risk of ASD by aggravating pathological motility compensation of the adjacent segment. To confirm this hypothesis, we simulated S-A oblique lumbar interbody fusion (OLIF) and OLIF with BPS fixation in well-validated finite element (FE) models with different BMDs. ROMs and stiffness in both surgical and adjacent segments were computed and recorded to identify surgical segment stability and motility compensation of the adjacent segments.

Methods

Model construction and validation

We simulated S-A OLIF and OLIF with BPS fixation in a well-validated FE lumbosacral model. In this process, we performed a multi-indicator model validation to verify the computational credibility of the FE model (16, 17). To construct bony structures, reconstructed bony outlines were inputted into 3D CAD software, and outlines of bony structures were drawn by fitted curves to construct bony structures with fitted surfaces. In this process, bony structures, including cortical, cancellous, and bony endplates, were constructed separately. The cortical thickness was set to 0.5 mm, and the thickness, concave angles, and depth in both coronal and sagittal planes were defined according to the measurements of imaging data and anatomical samples (18–20). Nonbony components were constructed in the same 3D CAD software. IVD components comprise the annulus,

nucleus, and CEPs, and the outline of the CEP covers the nucleus and inner parts of the annulus (21, 22). Facet cartilages were defined as contact-to-contact surfaces, and ligament structures were defined as cable elements (23, 24). To validate whether the current model represents actual biomechanical situations, computed intradiscal pressure, facet contact force, disc compression value, and different directional ROMs were calculated and compared with the average values of the indicators recorded in in-vitro tests. Given that the differences between the computed and tested values were less than one standard deviation, we believe that the current model adequately represents actual biomechanical situations and can be used in current surgical simulations.

Surgical simulations

We performed OLIF simulations in the L4–L5 IVD because of the highest incidence of LDDs in this motion segment. The length of the OLIF cage was defined according to the measurement of

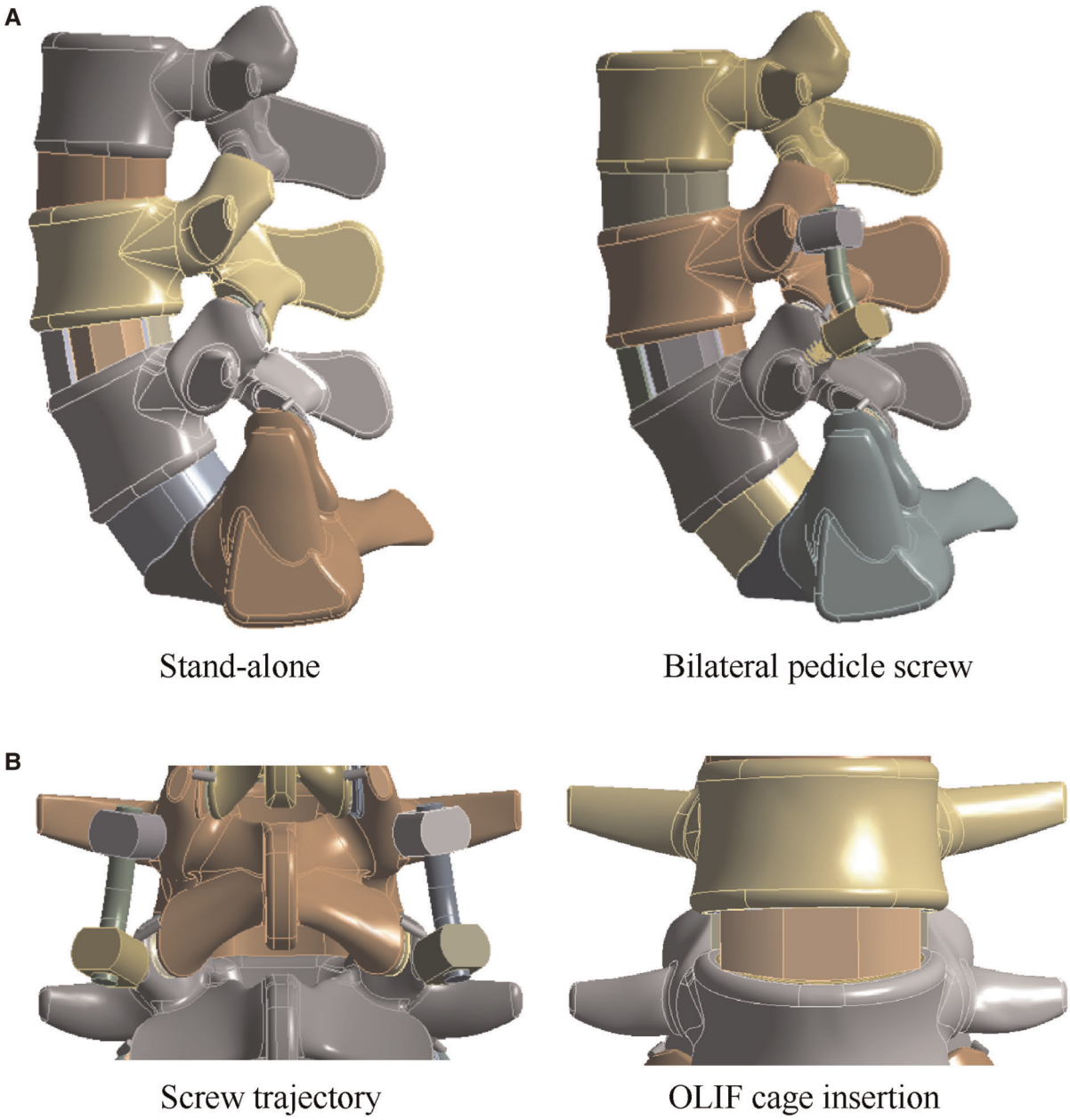

FIGURE 1
Schematic for surgical simulations in the lumbo-sacral model. (**A**) The intact lumbo-sacral model; (**B**) Simulations for S-A OLIF and OLIF fifixed by BPS.

TABLE 1 Material properties of FE models' components.

Components	Elastic modulus (MPa)	Poisson's ratio	Cross-section (mm^2)
Cortical (normal BMD)	E_{xx} = 11,300 E_{yy} = 11,300 E_{zz} = 22,000 G_{xy} = 3,800 G_{yz} = 5,400 G_{xz} = 5,400	V_{xy} = 0.484 V_{yz} = 0.203 V_{xz} = 0.203	
Cancellous (normal BMD)	E_{xx} = 140 E_{yy} = 140 E_{zz} = 200 G_{xy} = 48.3 G_{yz} = 48.3 G_{xz} = 48.3	V_{xy} = 0.45 V_{yz} = 0.315 V_{xz} = 0.315	
Bony endplates (normal BMD)	12,000	0.3	
Cortical (slight reduction of BMD)	Exx = 9,436 Eyy = 9,436 Ezz = 18,370 Gxy = 3,173 Gyz = 4,509 Gxz = 4,509	Vxy = 0.484 Vyz = 0.203 Vxz = 0.203	
Cancellous (slight reduction of BMD)	Exx = 93.8 Eyy = 93.8 Ezz = 150 Gxy = 32.36 Gyz = 36.23 Gxz = 36.23	Vxy = 0.45 Vyz = 0.315 Vxz = 0.315	
Bony endplates (slight reduction of BMD)	10,035	0.3	
Cortical (significant reduction of BMD)	Exx = 7,571 Eyy = 7,571 Ezz = 14,740 Gxy = 2,546 Gyz = 3,618 Gxz = 3,618	Vxy = 0.484 Vyz = 0.203 Vxz = 0.203	
Cancellous (significant reduction of BMD)	Exx = 47.6 Eyy = 47.6 Ezz = 100 Gxy = 16.42 Gyz = 24.15 Gxz = 24.15	Vxy = 0.45 Vyz = 0.315 Vxz = 0.315	
Bony endplates (significant reduction of BMD)	8,070	0.3	
Annulus	Hypoelastic material		
Nucleus	1	0.49	
Cartilage endplates	10	0.4	
Anterior longitudinal ligaments	Calibrated load-deformation curved under different loading conditions	0.3	60
Posterior longitudinal ligaments	Calibrated load-deformation curved under different loading conditions	0.3	21
Ligamentum flavum	Calibrated load-deformation curved under different loading conditions	0.3	60
Interspinous ligaments	Calibrated load-deformation curved under different loading conditions	0.3	40
Supraspinous ligaments	Calibrated load-deformation curved under different loading conditions	0.3	30
Intertransverse ligaments	Calibrated load-deformation curved under different loading conditions	0.3	10
Capsular	7.5 (25%) 32.9 (25%)	0.3	67.5
PEEK OLIF cage	3,500	0.3	
Titanium alloy screw	110,000	0.3	

vertebral body sizes. An OLIF cage model of 50 mm length was constructed in the same 3D CAD software. The nucleus, CEPs, and two lateral sides of the annulus were removed to simulate the discectomy and endplate preparation, and the OLIF cage fully covered with GB was inserted into the interbody space (**Figure 1**) (25, 26). The long axis of the OLIF cage was parallel to the coronal plane of the lumbosacral models. The height of the interbody space and lordotic angles of the surgical segment were kept identical to the corresponding postoperative models to eliminate their biomechanical effects (26, 27). S-A OLIF simulations were accomplished by performing these procedures. For simulating percutaneous BPS fixation, cannulated pedicle screw models of 6.5 mm diameter were constructed. Four identical pedicle screws were inserted into the L4 and L5 vertebral bodies (**Figure 1**) (28, 29).

Boundary and loading conditions

The boundary and loading conditions of the current models were defined according to *in vitro* biomechanical tests. The inferior surfaces of S1 were completely fixed, while different directional moments were applied to the superior surfaces of L3 (8, 21). Models were computed under identical loading conditions, including 8 Nm flexion, 6 Nm extension and bending, and 4 Nm axial rotation (30, 31). Because current models are symmetrical in the central sagittal plane alone, bending and axial rotation loading

conditions can be computed unilaterally. The contact between facet cartilages was set as frictionless. The frictional coefficient between the OLIF cage and BEPs was set as 0.2, and that between the GB and BEPs was set as 0.46 to simulate the instant postoperative biomechanical environment (32, 33).

Mesh generation strategies used in the present study were consistent with those reported in our previous studies, and the mesh convergence test was also performed to eliminate the effect of mesh size on the biomechanical performance of the models (16, 17). The annulus was defined as a hypoelastic material, and the nucleus was set as a semifluid incompressible bag (15, 34). Pedicle screw material was defined as titanium alloy (Ti6Al4 V), and the OLIF cage was defined as polyether ether ketone (PEEK); the elastic modulus of the GB was calculated based on the measurement of Hounsfield unit (HU) values immediately after the CT scan (34, 35). The material properties of cortical and cancellous bones were defined according to anisotropic laws, and BEP was set as an isotropic material (36, 37). For constructing postoperative models with normal BMD, osteopenia, and osteoporosis, the stiffness of cortical, cancellous, and BEPs was adjusted according to the same numerical simulations and tests used for bony material properties (**Table 1**). The morphological parameters of bony structures remained unchanged (37–39).

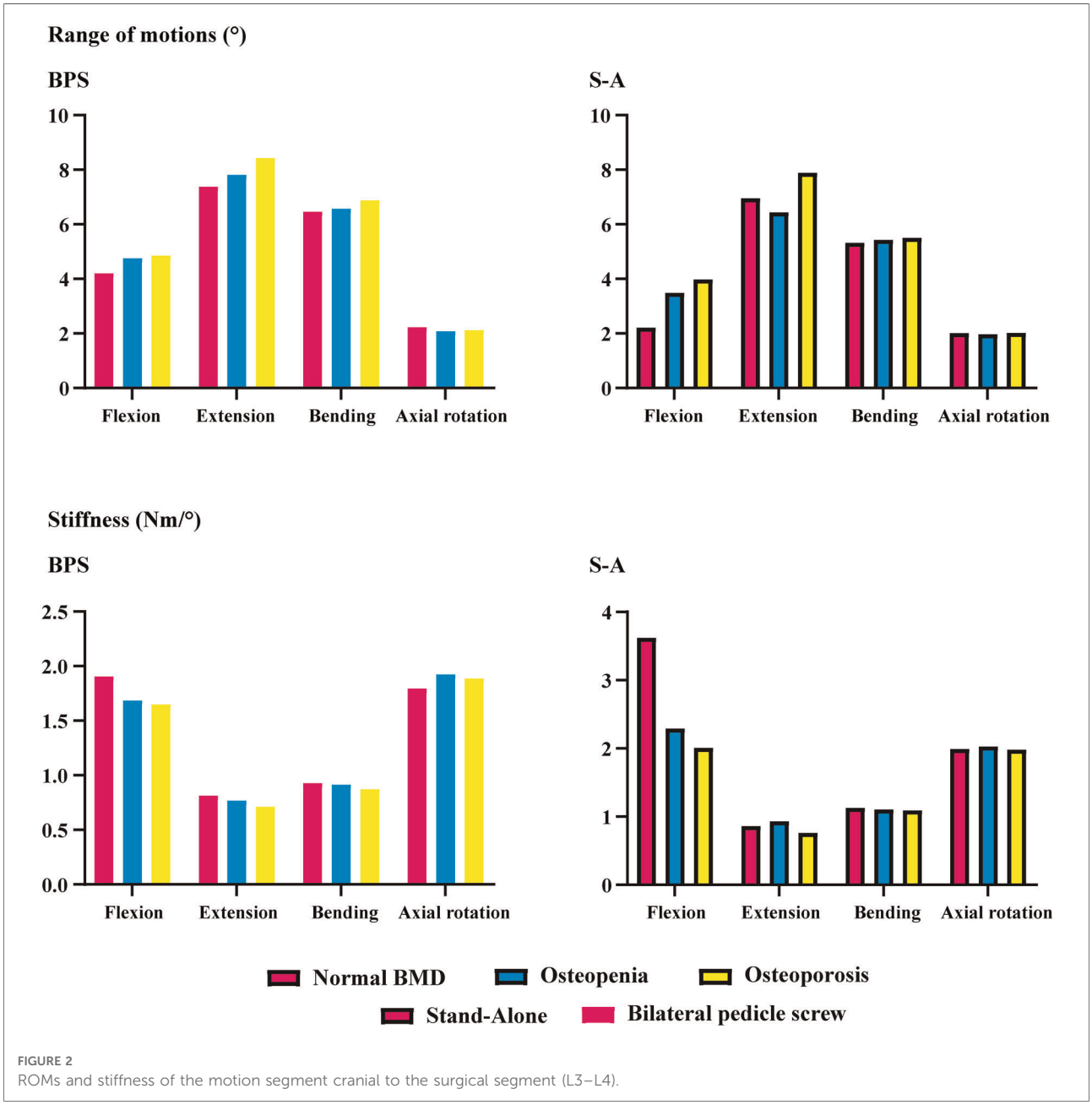

FIGURE 2
ROMs and stiffness of the motion segment cranial to the surgical segment (L3–L4).

Results

Motility compensation of adjacent segments in models with different BMDs

ROMs and stiffness in adjacent segments were computed and recorded in the present study. Both cranial and caudal motion segments exhibited identical overall variation. Specifically, one step decrease in BMD aggravated motility compensation (i.e., ROMs increased and stiffness decreased with the decrease in the bony elastic modulus). Contrary to the common belief, motility compensation was greater on the caudal side than on the cranial side in both BPS and S-A models. Under the flexion loading condition, the most significant motility compensation was observed in S-A models. Compared to the model with normal BMD, ROMs increased by nearly 80% in both cranial and caudal side motion segments (Figures 2, 3).

Only a few exceptions were observed in osteopenia models under axial rotation loading conditions, in which ROMs decreased by 6.73% and 1.99% in BPS and S-A OLIF models, respectively, and decreased by 4.93% in the osteoporosis model with BPS fixation. In addition, under the extension loading condition of BPS models, ROMs increased by 47.35% and 15.99% in osteopenia and osteoporosis models, respectively; compared to osteoporosis models, this was the

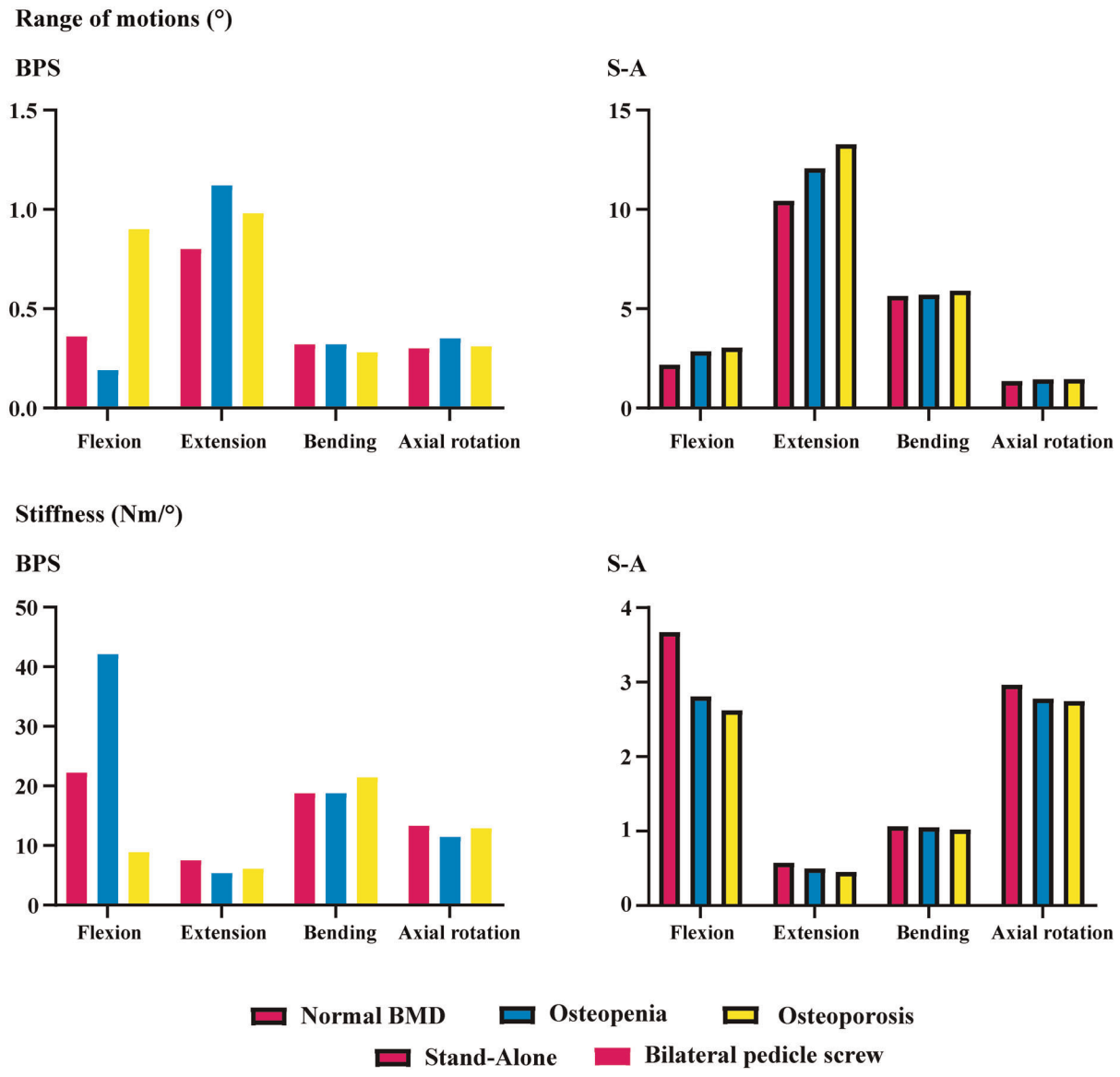

FIGURE 3
ROMs and stiffness of the motion segment caudal to the surgical segment (L5–S1).

only loading condition in which the motility compensation was more severe in osteopenia models (Figures 2, 3).

Instantly postoperative stability in the surgical segment

BPS models showed smaller ROMs and higher stiffness in the surgical segment than S-A models. Under the flexion and axial rotation loading conditions, the ROMs of the S-A models were smaller than 3°, except for the osteoporosis model, whose ROM was slightly larger than 3° under the flexion loading condition. In contrast, poor instant postoperative stability of S-A models was observed under extension and lateral bending loading conditions, in which ROMs were larger than 5° under bending and even larger than 10° under extension loading conditions. As shown in the nephograms, apparent separations were observed between the BEPs and OLIF cage in the S-A models under extension and bending loading conditions (Figures 4, 5).

Discussion

To investigate the biomechanical effects of BMD reduction on motility compensation of segments adjacent to the LIF

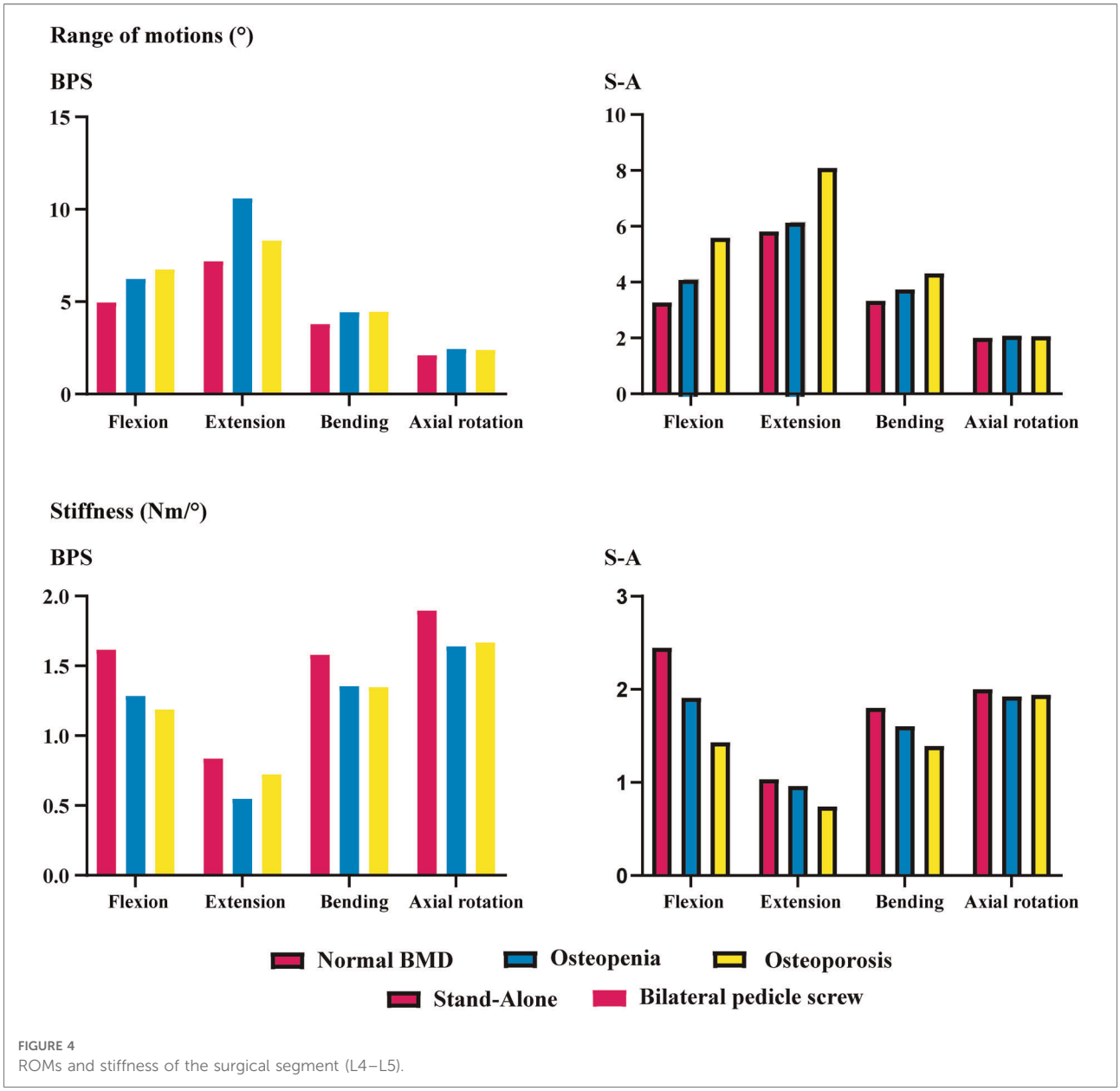

FIGURE 4
ROMs and stiffness of the surgical segment (L4–L5).

10.3389/fsurg.2022.967399

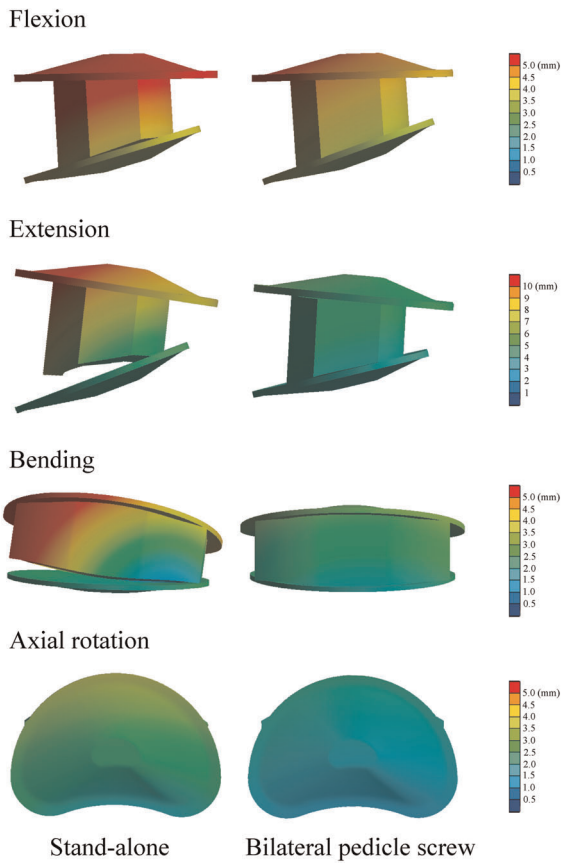

FIGURE 5
Nephograms for BEPs and the OLIF cage under different loading conditions.

operative segment, S-A OLIF and OLIF with BPS fixation were simulated in well-validated lumbosacral FE models with different BMDs. Computational results showed that the decrease in BMD leads to severe motility compensation of both cranial and caudal adjacent segments. This may be a reasonable explanation for the higher incidence of ASD in patients with poor BMD after LIF surgeries.

ASD is a widely reported complication after LIF surgeries. The recurrence of symptoms and the resulting reoperations adversely affect the clinical outcomes of patients. Biomechanical deterioration is an important cause of ASD (40, 41). Stress concentration and motility compensation are two types of biomechanical deterioration. Specifically, LIF surgery induces stress concentration in adjacent segments' IVDs and facet cartilages of zygapophyseal joints (ZJs). These changes increase the incidence of annular tears and cause acceleration of DD and degenerative osteoarthritis of ZJs (6, 23). These pathological changes are common types of ASDs. Additionally, LIF surgeries increase the stiffness of the surgical segment (decrease ROMs under the same sizes of moments). Thus, during daily activities, the reduced ROMs of the surgical segment should be compensated by adjacent segments, which is also a common cause of ASD (3, 4, 9).

In the present study, the extent of motility compensation of adjacent segments steeply increased with the decrease in bony elastic modulus. This computational result partially explains the reason why patients with osteoporosis have a high risk of ASD biomechanically. Moreover, regular antiosteoporosis therapy is recommended in osteoporotic patients after LIF surgery. Generally, surgeons believe that this patient management strategy could reduce the incidence of surgical segment complications (e.g., screw loosening and cage subsidence). On the basis of current computational results, the significance of postoperative anti-osteoporosis has been further emphasized, and we believe that it could optimize clinical outcomes of patients by reducing the risk of both surgical segment and adjacent segment complications.

The pathological process of stress concentration in adjacent segments after LIF surgery has been widely reported. Previous studies have shown that the incidence rate of ASD in the segment cranial to the surgical segment was higher than that in the caudal segment, and the biomechanical mechanism of this phenomenon was the shorter force arm, resulting in higher grades of stress concentration of the cranial side IVD (5, 6, 15). However, the variation in motility compensation was inconsistent with stress concentrations. In the present study, the variation in motility compensation in the caudal segment was overall comparable to that in the cranial segment and even more pronounced in the caudal segment under some loading conditions. Considering the exact effect of motility compensation on the risk of ASD, the incidence of ASD on the caudal side adjacent segment should not be ignored in future clinical studies (**Figures 2**, **3**).

The difference in instant postoperative stability between S-A OLIF and OLIF with BPS fixation was also compared. Consistent with the consensus, as the gold standard of AFD, BPS fixation provides excellent fixation stability (13, 42). However, the apparent separation between the OLIF cage and BEPs in the S-A models was considered for daily size moments (especially under extension and lateral bending loading conditions) (**Figure 5**). Therefore, although the BPS models show more severe motility compensation, we recommend using AFDs in OLIF patients to reduce the incidence of complications related to the separation between BEPs and the OLIF cage (e.g., cage migrations and nonunions). We also recommend restricting daily motions or AFDs (e.g., semirigid waistline) in S-A patients in the early postoperative period to reduce complication risk.

In conclusion, although no consensus was noted on the relationship between poor BMD and ASD incidence by computing stress concentration grades in adjacent segment IVDs and ZJs, a clear variation in motility compensation was observed in current models, and a reasonable explanation can be derived from the biomechanical perspective.

Specifically, following the reduction in bony BMD, differences in stiffness between the LIF motion segment with insertional devices (e.g., OLIF cage, GB, and AFDs) and adjacent segment IVDs and more severe motility compensation can be deduced.

The conclusion of this study should be accepted only after acknowledging the following limitations. As an inherent defect of FE studies, the present study could not simulate *in vivo* biological and morphological changes during the interbody fusion process. Therefore, it is difficult to simulate the influence of BEP damage, cage subsidence, and screw loosening on adjacent segments of biomechanical environments. More significantly, spinal instability could induce *in vivo* self-adaptation mechanics, leading to the generation of osteophytes that affect local biomechanical environments, which was also ignored in this study (43, 44). We hope to address these limitations in future studies by further calibration and optimization of FE models.

Conclusion

Poor BMD aggravates the motility compensation of the adjacent segment after S-A OLIF and OLIF with BPS fixation; this variation may increase the incidence of ASD. The S-A surgical method cannot provide instant postoperative stability; hence, daily motions of S-A patients should be restricted, or AFDs (e.g., semirigid waistline) should be used in the early postoperative period to avoid surgical segment complications.

Data availability statement

The original contributions presented in the study are included in the article/Supplementary Material, further inquiries can be directed to the corresponding author/s.

Ethics statement

The studies involving human participants were reviewed and approved by Approval for the current study protocol (including the lumbar CT scan) was obtained from the ethics committees of Jiangsu Province Hospital on Integration of Chinese and Western Medicine (2019LWKY015). We confirm that the subject signed the informed consent and submitted it to the ethics committee for review before the examination, and all methods were carried out in accordance with relevant guidelines and regulations. Written informed consent for participation was not required for this study in accordance with the national legislation and the institutional requirements.

Author contributions

Conception and design: J-CL, Z-PX, and C-YH; Model construction and finite element analysis: J-CL, Z-XF, and C-YH; Analysis and interpretation of data: C-YH, Z-FZ, FL, and J-CL; Figures preparation: Z-FZ, C-YH, X-YZ, and Z-PX; Manuscript Preparation and modification: C-YH, Z-FZ, Z-PX, and J-CL. All authors contributed to the article and approved the submitted version.

Funding

This study was supported by the project of applied basic research in the Southwest Medical University (2021ZKQN129) and the Hejiang County People's Hospital —Southwest Medical University Cooperative project (2021HJXNYD08).

Conflict of interest

The remaining authors declare that the research was conducted in the absence of any commercial or financial relationships that could be construed as a potential conflict of interest. The reviewer WY declared a shared affiliation with the author ZFZ to the handling editor at the time of review.

Publisher's note

All claims expressed in this article are solely those of the authors and do not necessarily represent those of their affiliated organizations, or those of the publisher, the editors and the reviewers. Any product that may be evaluated in this article, or claim that may be made by its manufacturer, is not guaranteed or endorsed by the publisher.

References

1. Cappuccino A, Cornwall GB, Turner AW, Fogel GR, Duong HT, Kim KD, et al. Biomechanical analysis and review of lateral lumbar fusion constructs. *Spine*. (2010) 35(26 Suppl):S361–7. doi: 10.1097/BRS.0b013e318202308b

2. Faizan A, Kiapour A, Kiapour AM, Goel VK. Biomechanical analysis of various footprints of transforaminal lumbar interbody fusion devices. *J Spinal Disord Tech*. (2014) 27(4):E118–27. doi: 10.1097/BSD.0b013e3182a11478

3. Park P, Garton HJ, Gala VC, Hoff JT, McGillicuddy JE. Adjacent segment disease after lumbar or lumbosacral fusion: review of the literature. *Spine*. (2004) 29(17):1938–44. doi: 10.1097/01.brs.0000137069.88904.03

4. Wang H, Ma L, Yang D, Wang T, Liu S, Yang S, et al. Incidence and risk factors of adjacent segment disease following posterior decompression and instrumented fusion for degenerative lumbar disorders. *Medicine (Baltimore)*. (2017) 96(5):e6032. doi: 10.1097/md.0000000000006032

5. Hsieh YY, Tsuang FY, Kuo YJ, Chen CH, Chiang CJ, Lin CL. Biomechanical analysis of single-level interbody fusion with different internal fixation rod materials: a finite element analysis. *BMC Musculoskelet Disord*. (2020) 21 (1):100. doi: 10.1186/s12891-020-3111-1

6. Hsieh YY, Chen CH, Tsuang FY, Wu LC, Lin SC, Chiang CJ. Removal of fixation construct could mitigate adjacent segment stress after lumbosacral fusion: a finite element analysis. *Clin Biomech (Bristol, Avon)*. (2017) 43:115–20. doi: 10.1016/j.clinbiomech.2017.02.011

7. Zhu G, Hao Y, Yu L, Cai Y, Yang X. Comparing stand-alone oblique lumbar interbody fusion with posterior lumbar interbody fusion for revision of rostral adjacent segment disease: a STROBE-compliant study. *Medicine (Baltimore)*. (2018) 97(40):e12680. doi: 10.1097/md.0000000000012680

8. Li J, Xu W, Zhang X, Xi Z, Xie L. Biomechanical role of osteoporosis affects the incidence of adjacent segment disease after percutaneous transforaminal endoscopic discectomy. *J Orthop Surg Res*. (2019) 14(1):131. doi: 10.1186/s13018-019-1166-1

9. Lee JC, Kim Y, Soh JW, Shin BJ. Risk factors of adjacent segment disease requiring surgery after lumbar spinal fusion: comparison of posterior lumbar interbody fusion and posterolateral fusion. *Spine*. (2014) 39(5):E339–45. doi: 10.1097/brs.0000000000000164

10. Qasim M, Natarajan RN, An HS, Andersson GB. Damage accumulation location under cyclic loading in the lumbar disc shifts from inner annulus lamellae to peripheral annulus with increasing disc degeneration. *J Biomech*. (2014) 47(1):24–31. doi: 10.1016/j.jbiomech.2013.10.032

11. Bydon M, Macki M, Kerezoudis P, Sciubba DM, Wolinsky JP, Witham TF, et al. The incidence of adjacent segment disease after lumbar discectomy: a study of 751 patients. *J Clin Neurosci*. (2017) 35:42–6. doi: 10.1016/j.jocn.2016.09.027

12. Zhang C, Shi J, Chang M, Yuan X, Zhang R, Huang H, et al. Does osteoporosis affect the adjacent segments following anterior lumbar interbody fusion? A finite element study. *World Neurosurg*. (2020) 146:e739–46. doi: 10.1016/j.wneu.2020.11.005

13. Guo HZ, Tang YC, Guo DQ, Luo PJ, Li YX, Mo GY, et al. Stability evaluation of oblique lumbar interbody fusion constructs with Various fixation options: a finite element analysis based on three-dimensional scanning models. *World Neurosurg*. (2020) 138:e530–8. doi: 10.1016/j.wneu.2020.02.180

14. Reis MT, Reyes PM, Bse AI, Newcomb AG, Singh V, Chang SW, et al. Biomechanical evaluation of lateral lumbar interbody fusion with secondary augmentation. *J Neurosurg Spine*. (2016) 25(6):720–6. doi: 10.3171/2016.4.Spine151386

15. Kim HJ, Chun HJ, Moon SH, Kang KT, Kim HS, Park JO, et al. Analysis of biomechanical changes after removal of instrumentation in lumbar arthrodesis by finite element analysis. *Med Biol Eng Comput*. (2010) 48(7):703–9. doi: 10.1007/s11517-010-0621-2

16. Li J, Xu C, Zhang X, Xi Z, Sun S, Zhang K, et al. Disc measurement and nucleus calibration in a smoothened lumbar model increases the accuracy and efficiency of in-silico study. *J Orthop Surg Res*. (2021) 16(1):498. doi: 10.1186/s13018-021-02655-4

17. Li JC, Xie TH, Zhang Z, Song ZT, Song YM, Zeng JC. The mismatch between bony endplates and grafted bone increases screw loosening risk for OLIF patients with ALSR fixation biomechanically. *Front Bioeng Biotechnol*. (2022) 10:862951. doi: 10.3389/fbioe.2022.862951

18. Liu JT, Han H, Gao ZC, He CY, Cai X, Niu BB, et al. CT Assisted morphological study of lumbar endplate. *Chin J Orthop Trauma*. (2018) 31(12) :1129–35. doi: 10.3969/j.issn.1003-0034.2018.12.011

19. Pan CL, Zhang BY, Zhu YH, Ma YH, Li MF, Wang X, et al. Morphologic analysis of Chinese lumbar endplate by three-dimensional computed tomography reconstructions for helping design lumbar disc prosthesis. *Medicine (Baltimore)*. (2021) 100(6):e24583. doi: 10.1097/md.0000000000024583

20. Zhao FD, Pollintine P, Hole BD, Adams MA, Dolan P. Vertebral fractures usually affect the cranial endplate because it is thinner and supported by less-dense trabecular bone. *Bone*. (2009) 44(2):372–9. doi: 10.1016/j.bone.2008.10.048

21. Li J, Zhang X, Xu W, Xi Z, Xie L. Reducing the extent of facetectomy may decrease morbidity in failed back surgery syndrome. *BMC Musculoskelet Disord*. (2019) 20(1):369. doi: 10.1186/s12891-019-2751-5

22. Xu C, Xi Z, Fang Z, Zhang X, Wang N, Li J, et al. Annulus calibration increases the computational accuracy of the lumbar finite element model. *Global Spine J*. (2022):21925682221081224. doi: 10.1177/21925682221081224

23. Chuang WH, Lin SC, Chen SH, Wang CW, Tsai WC, Chen YJ, et al. Biomechanical effects of disc degeneration and hybrid fixation on the transition and adjacent lumbar segments: trade-off between junctional problem, motion preservation, and load protection. *Spine*. (2012) 37(24):E1488–97. doi: 10.1097/BRS.0b013e31826cdd93

24. Chuang WH, Kuo YJ, Lin SC, Wang CW, Chen SH, Chen YJ, et al. Comparison among load-, ROM-, and displacement-controlled methods used in the lumbosacral nonlinear finite-element analysis. *Spine*. (2013) 38(5):E276–85. doi: 10.1097/BRS.0b013e31828251f9

25. Lu T, Lu Y. Comparison of biomechanical performance among posterolateral fusion and transforaminal, extreme, and oblique lumbar interbody fusion: a finite element analysis. *World Neurosurg*. (2019) 129:e890–9. doi: 10.1016/j.wneu.2019.06.074

26. Wang B, Hua W, Ke W, Lu S, Li X, Zeng X, et al. Biomechanical evaluation of transforaminal lumbar interbody fusion and oblique lumbar interbody fusion on the adjacent segment: a finite element analysis. *World Neurosurg*. (2019) 126:e819–24. doi: 10.1016/j.wneu.2019.02.164

27. Kim HJ, Chun HJ, Kang KT, Moon SH, Kim HS, Park JO, et al. The biomechanical effect of pedicle screws' insertion angle and position on the superior adjacent segment in 1 segment lumbar fusion. *Spine*. (2012) 37 (19):1637–44. doi: 10.1097/BRS.0b013e31823f2115

28. Liu JM, Zhang Y, Zhou Y, Chen XY, Huang SH, Hua ZK, et al. The effect of screw tunnels on the biomechanical stability of vertebral body after pedicle screws removal: a finite element analysis. *Int Orthop*. (2017) 41(6):1183–7. doi: 10.1007/s00264-017-3453-y

29. Chao CK, Hsu CC, Wang JL, Lin J. Increasing bending strength and pullout strength in conical pedicle screws: biomechanical tests and finite element analyses. *J Spinal Disord Tech*. (2008) 21(2):130–8. doi: 10.1097/BSD.0b013e318073cc4b

30. Kim HJ, Kang KT, Son J, Lee CK, Chang BS, Yeom JS. The influence of facet joint orientation and tropism on the stress at the adjacent segment after lumbar fusion surgery: a biomechanical analysis. *Spine J*. (2015) 15(8):1841–7. doi: 10.1016/j.spinee.2015.03.038

31. Kim HJ, Kang KT, Chun HJ, Lee CK, Chang BS, Yeom JS. The influence of intrinsic disc degeneration of the adjacent segments on its stress distribution after one-level lumbar fusion. *Eur Spine J*. (2015) 24(4):827–37. doi: 10.1007/s00586-014-3462-0

32. Polikeit A, Ferguson SJ, Nolte LP, Orr TE. Factors influencing stresses in the lumbar spine after the insertion of intervertebral cages: finite element analysis. *Eur Spine J*. (2003) 12(4):413–20. doi: 10.1007/s00586-002-0505-8

33. Zhong ZM, Deviren V, Tay B, Burch S, Berven SH. Adjacent segment disease after instrumented fusion for adult lumbar spondylolisthesis: incidence and risk factors. *Clin Neurol Neurosurg*. (2017) 156:29–34. doi: 10.1016/j.clineuro.2017.02.020

34. Xu C, Huang C, Cai P, Fang Z, Wei Z, Liu F, et al. Biomechanical effects of pedicle screw positioning on the surgical segment in models after oblique lumbar interbody fusion: an in-silico study. *Int J Gen Med*. (2022) 15:1047–56. doi: 10.2147/ijgm.S352304

35. Takenaka S, Kaito T, Ishii K, Watanabe K, Watanabe K, Shinohara A, et al. Influence of novel design alteration of pedicle screw on pull-out strength: a finite element study. *J Orthop Sci*. (2020) 25(1):66–72. doi: 10.1016/j.jos.2019.03.002

36. Morgan EF, Bayraktar HH, Keaveny TM. Trabecular bone modulus-density relationships depend on anatomic site. *J Biomech*. (2003) 36(7):897–904. doi: 10.1016/s0021-9290(03)00071-x

37. Tsouknidas A, Sarigiannidis SO, Anagnostidis K, Michailidis N, Ahuja S. Assessment of stress patterns on a spinal motion segment in healthy versus osteoporotic bony models with or without disc degeneration: a finite element analysis. *Spine J*. 2015;15(3 Suppl):S17–22. doi: 10.1016/j.spinee.2014.12.148

38. Polikeit A, Nolte LP, Ferguson SJ. The effect of cement augmentation on the load transfer in an osteoporotic functional spinal unit: finite-element analysis. *Spine*. (2003) 28(10):991–6. doi: 10.1097/01.Brs.0000061987.71624.17

39. Zhang L, Yang G, Wu L, Yu B. The biomechanical effects of osteoporosis vertebral augmentation with cancellous bone granules or bone cement on treated and adjacent non-treated vertebral bodies: a finite element evaluation. *Clin Biomech (Bristol, Avon)*. (2010) 25(2):166–72. doi: 10.1016/j.clinbiomech.2009.10.006

40. Tsuang FY, Tsai JC, Lai DM. Effect of lordosis on adjacent levels after lumbar interbody fusion, before and after removal of the spinal fixator: a finite element analysis. *BMC Musculoskelet Disord*. (2019) 20(1):470. doi: 10.1186/s12891-019-2886-4

41. Ruberté LM, Natarajan RN, Andersson GB. Influence of single-level lumbar degenerative disc disease on the behavior of the adjacent segments–a finite element model study. *J Biomech.* (2009) 42(3):341–8. doi: 10.1016/j.jbiomech.2008.11.024

42. Doulgeris JJ, Aghayev K, Gonzalez-Blohm SA, Lee WE, Vrionis FD. Biomechanical comparison of an interspinous fusion device and bilateral pedicle screw system as additional fixation for lateral lumbar interbody fusion. *Clin Biomech (Bristol, Avon).* (2015) 30(2):205–10. doi: 10.1016/j.clinbiomech.2014.10.003

43. Galbusera F, van Rijsbergen M, Ito K, Huyghe JM, Brayda-Bruno M, Wilke HJ. Ageing and degenerative changes of the intervertebral disc and their impact on spinal flexibility. *Eur Spine J.* (2014) 23(Suppl 3):S324–32. doi: 10.1007/s00586-014-3203-4

44. Pye SR, Reid DM, Adams JE, Silman AJ, O'Neill TW. Radiographic features of lumbar disc degeneration and bone mineral density in men and women. *Ann Rheum Dis.* (2006) 65(2):234–8. doi: 10.1136/ard.2005.038224